Analysis of Hydrogen Maser Frequency Drift Due to Possible Drifts in Load VSWR and Phase Angle of Reflection Coefficient

R. W. Beatty[1] and T. Y. Otoshi
Radio Frequency and Microwave Subsystems Section

Theoretical equations are derived for calculating the effects of load VSWR and reflection coefficient phase-angle drifts on hydrogen maser frequency stability. Sample calculations made for a typical JPL maser show that under special load conditions, a VSWR drift of 7.5×10^{-5}/h or phase angle drift of 0.015 deg/h can produce a frequency drift of $(10^{-14} f_0)$ Hz/h where f_0 is the maser frequency of approximately 1.42×10^9 Hz.

I. Introduction

It is well known that the frequency of a hydrogen maser oscillator can be pulled by the loading on its cavity. In applications requiring especially good frequency stability of a microwave source, such as in VLBI (very long baseline interferometry), very small load changes can cause significant frequency variations or drifts. In the following, this situation is analyzed in order to determine maximum drift sensitivity factors in a particular case.

II. Analysis

The case under consideration is shown in the simplified diagram of Fig. 1. The virtual resonant circuit located at the reference plane is shown.

The following familiar equations apply (for example, Ref. 1).

$$\left.\begin{aligned} Q_u &= \frac{\omega C}{G}, \quad Q_L = \frac{\omega C}{G + G_L} \\ Q_C &= \frac{\omega C}{G_L}, \quad Q_E = \frac{\omega C}{Y_0} \\ \beta &= \frac{Q_u}{Q_E} = \frac{Y_0}{G} \end{aligned}\right\} \qquad (1)$$

where Q_U, Q_L are respectively the unloaded and loaded Q of the cavity; Q_C, Q_E are respectively the coupled and external Q; β is the coupling factor; and as shown in Fig. 1, G and G_L are the cavity and load conductances, respectively, and Y_0 is the characteristic admittance of the transmission line. It is

[1] R. W. Beatty is a consulting electronics engineer at 2110 Fourth Street, Boulder, CO 80302.

assumed in the above that Y_0 is positive real (i.e., $Y_0 = G_0$). Under loaded conditions, the resonant frequency of the cavity is given by

$$f_L = \frac{1}{2\pi \sqrt{L(C + C_L)}} \tag{2}$$

where the L and C are, respectively, the inductance and capacitance elements of the cavity shown in Fig. 1, and C_L is the equivalent load capacitance such that $B_L = \omega C_L$.

When the load is non-reactive ($B_L = 0$, $C_L = 0$), the cavity resonant frequency is

$$f = \frac{1}{2\pi \sqrt{LC}} \tag{3}$$

Let

$$\frac{\Delta f}{f} = \frac{f_L - f}{f} = \frac{f_L}{f} - 1 = \sqrt{\frac{C}{C + C_L}} - 1$$

$$\approx -\frac{C_L}{2C} \quad \text{for } C_L \ll C \tag{4}$$

Then

$$\frac{\Delta f}{f} \approx -\frac{\omega C_L}{2\omega C} = \frac{-B_L}{2\omega C} = -\frac{B_L}{Y_0}\left(\frac{1}{2Q_E}\right) \tag{5}$$

The hydrogen maser output frequency is pulled from the hydrogen line resonance by an amount that is proportional to the cavity resonant frequency shift according to the relationship (Ref. 2):

$$\Delta f_{\text{osc}} = \left(\frac{Q_L}{Q_H}\right) \Delta f \tag{6}$$

where Q_H is the Q of the hydrogen line. If we define f_0 to be the hydrogen line resonant frequency and $\delta = f - f_0$, then

$$\frac{\Delta f_{\text{osc}}}{f_0} = \left(\frac{Q_L}{Q_H}\right) \frac{\Delta f}{f\left(1 - \frac{\delta}{f}\right)} \approx \frac{Q_L}{Q_H}\left(\frac{\Delta f}{f}\right) \tag{7}$$

The above approximation is a good assumption because in practice, δ is normally made close to zero by adjustments made with a mechanical tuning slug in the cavity. From (1)

$$Q_L = \frac{\omega C}{G + G_L} = \frac{\frac{\omega C}{Y_0}}{\frac{G}{Y_0} + \frac{G_L}{Y_0}}$$

$$= \frac{Q_E}{\frac{1}{\beta} + \frac{G_L}{Y_0}} = \frac{\beta Q_E}{1 + \beta\left(\frac{G_L}{Y_0}\right)} \tag{8}$$

Then substitution into (7) gives

$$\frac{\Delta f_{\text{osc}}}{f_0} = \frac{\beta Q_E}{Q_H} \cdot \frac{1}{1 + \beta\left(\frac{G_L}{Y_0}\right)} \cdot \frac{\Delta f}{f} \tag{9}$$

Substitution of (5) gives

$$\frac{\Delta f_{\text{osc}}}{f_0} = -\frac{\beta}{2Q_H} \cdot \frac{\frac{B_L}{Y_0}}{1 + \beta\left(\frac{G_L}{Y_0}\right)} \tag{10}$$

We are interested in the rate of change or drift of $\Delta f_{\text{osc}}/f_0$ with time, or

$$\frac{d}{dt}\left(\frac{\Delta f_{\text{osc}}}{f_0}\right) = -\frac{\beta}{2Q_H} \cdot \frac{d}{dt}\left[\frac{\frac{B_L}{Y_0}}{1 + \beta\left(\frac{G_L}{Y_0}\right)}\right] \tag{11}$$

into which we may substitute

$$\frac{G_L}{Y_0} = \text{Re}\left(\frac{Y_L}{Y_0}\right) = \text{Re}\,\frac{1 - \Gamma_L}{1 + \Gamma_L} = \frac{1 - |\Gamma_L|^2}{|1 + \Gamma_L|^2} \tag{12}$$

$$\frac{B_L}{Y_0} = \mathrm{Im}\left(\frac{Y_L}{Y_0}\right) = \mathrm{Im}\,\frac{1-\Gamma_L}{1+\Gamma_L} = \frac{-2\,|\Gamma_L|\sin\psi_L}{|1+\Gamma_L|^2} \tag{13}$$

where $|\Gamma_L|$ and ψ_L are, respectively, the magnitude and phase angle of the load voltage reflection coefficient Γ_L at the reference plane shown in Fig. 1. For a general function F

$$\frac{d}{dt}F(|\Gamma_L|, \psi_L) = \left(\frac{\partial F}{\partial |\Gamma_L|}\right)\frac{d|\Gamma_L|}{dt} + \left(\frac{\partial F}{\partial \psi_L}\right)\frac{d\psi_L}{dt} \tag{14}$$

Hence

$$\frac{d}{dt}\left(\frac{\Delta f_{osc}}{f_0}\right) = \frac{\beta}{Q_H}\left\{\frac{[(1+\beta)-(1-\beta)|\Gamma_L|^2]\sin\psi_L}{[(1+\beta)+(1-\beta)|\Gamma_L|^2+2|\Gamma_L|\cos\psi_L]^2}\,\frac{d|\Gamma_L|}{dt}\right.$$

$$\left. + |\Gamma_L|\,\frac{[(1+\beta)+(1-\beta)|\Gamma_L|^2]\cos\psi_L + 2|\Gamma_L|}{[(1+\beta)+(1-\beta)|\Gamma_L|^2+2|\Gamma_L|\cos\psi_L]^2}\,\frac{d\psi_L}{dt}\right\} \tag{15}$$

This equation shows clearly the strong dependence of drift in oscillator frequency on the coupling coefficient β. If the cause of drift was in the load circuit or transmission line, a reduction in coupling would reduce it. Three other possible sources of oscillator frequency drift, not included in Eq. (15), are internal to the maser cavity and have been analyzed by Vessot, et al. (Ref. 2). Examination of their analysis reveals that if the cause of drift is in the maser cavity, a reduction in coupling would not lower the oscillator drift. Therefore, reduction of coupling factor would be one way to experimentally localize the source of frequency drift.

Although the differentiation was made with respect to time in Eq. (15), it could have been made with respect to any other variable. For example, if t in Eq. (15) were replaced by varactor voltage, one could arrive at the differential equation of the varactor tuning curve. Thus the above derivations have more general application than one might at first expect.

The load VSWR

$$\sigma_L = \frac{1+|\Gamma_L|}{1-|\Gamma_L|} \tag{16}$$

and

$$\frac{d\sigma_L}{dt} = \frac{2}{(1-|\Gamma_L|)^2}\,\frac{d|\Gamma_L|}{dt} \tag{17}$$

If $d\psi_L = 0$, the VSWR drift sensitivity is derived from Eq. (15) as

$$\frac{d\sigma_L}{dt} = \frac{2Q_H}{\beta}\left[\frac{d}{dt}\left(\frac{\Delta f_{osc}}{f_0}\right)\right]$$

$$\times\,\frac{[(1+\beta)+(1-\beta)|\Gamma_L|^2+2|\Gamma_L|\cos\psi_L]^2}{(1-|\Gamma_L|)^2\,[(1+\beta)-(1-\beta)|\Gamma_L|^2]\sin\psi_L} \tag{18}$$

If $d\sigma_L = 0$, the load phase angle drift sensitivity is derived from Eq. (15) as

$$\frac{d\psi_L}{dt} = \frac{Q_H}{\beta|\Gamma_L|}\left[\frac{d}{dt}\left(\frac{\Delta f_{osc}}{f_0}\right)\right]$$

$$\times\,\frac{[(1+\beta)+(1-\beta)|\Gamma_L|^2+2|\Gamma_L|\cos\psi_L]^2}{[(1+\beta)+(1-\beta)|\Gamma_L|^2]\cos\psi_L+2|\Gamma_L|} \tag{19}$$

For a given $|\Gamma_L|$ or σ_L, the drift sensitivities depend upon ψ_L, and can vary over wide ranges. The maximum values with respect to ψ_L are of interest, and are as follows.

Case I. If $d\psi_L = 0$, maximum sensitivity to VSWR drift occurs according to Eq. (15) when $\psi_L = \pm\pi/2$, then

$$\frac{d\sigma_L}{dt} = \pm\frac{2Q_H}{\beta}\left[\frac{d}{dt}\left(\frac{\Delta f_{osc}}{f_0}\right)\right]$$

$$\times\,\frac{[(1+\beta)+(1-\beta)|\Gamma_L|^2]^2}{(1-|\Gamma_L|)^2\,[(1+\beta)-(1-\beta)|\Gamma_L|^2]} \tag{20}$$

If we assume

$$Q_H = 10^9, \beta = 0.5, |\Gamma_L| = 0.1 \text{ and } \left[\frac{d}{dt}\left(\frac{\Delta f_{osc}}{f_0}\right)\right]$$

$$= 10^{-14}/\text{h},$$

then $d\sigma_L/dt = \pm 7.5 \times 10^{-5}$ per hour. Stated in another way, if $\psi_L = \pm \pi/2$, the VSWR drift must be kept to less than 7.5×10^{-5} per hour to keep the fractional frequency drift of the maser to less than 10^{-14}/h.

Case II. If $d\,|\Gamma_L| = 0$, maximum sensitivity to load phase angle drift occurs according to Eq. (15) when $\psi_L = \pi, 3\pi$, etc. Then

$$\frac{d\psi_L}{dt} = \frac{-Q_H}{\beta|\Gamma_L|}\left[\frac{d}{dt}\left(\frac{\Delta f_{osc}}{f_0}\right)\right]\left[(1+\beta) + (1-\beta)|\Gamma_L|^2 - 2|\Gamma_L|\right] \tag{21}$$

If we assume the same parameters as in Case I, then,

$$\left|\frac{d\psi_L}{dt}\right| = 2.61 \times 10^{-4} \text{ radians per hour,}$$

$$\text{or } \cong 0.015 \text{ deg per hour}$$

III. Application to Specific Circuit

As shown in Fig. 2, a maser is electronically tuned by varying the bias on a varactor connected to reflect energy back to the maser through a directional coupler. Assuming that the varactor is lossless, it acts like a variable capacitance. The locus of its reflection coefficient is a segment of the unit circle as shown in Fig. 3.

Both the signal incident upon the varactor and its reflected signal are attenuated or decoupled from the main line by the directional coupler. If the coupling is 10 dB for example, the varactor will produce $|\Gamma_L| = 0.1$ in the main line, and the locus of the varactor reflection coefficient variation will appear as in Fig. 4. Note that the small reflection coefficient circle has a radius of 0.1, and that it has rotated due to the delay along the path from the reference plane in the main line to the varactor. As we visualize the effect of different path lengths, we can see that for some lengths, the locus line cuts across lines of constant susceptance and causes maximum frequency change, but for other lengths the locus line produces no change in susceptance or in frequency. Normally, a path length is selected experimentally for which nearly maximum *change* in load susceptance is produced by the varactor. Any drift in varactor bias, for example, would produce a drift in phase ψ_L and the sensitivity would correspond to that calculated from Eq. (21).

IV. Effect of Fixed Reflections

In the absence of reflections other than from the varactor, the small reflection coefficient circle shown in Fig. 4 is centered on the origin. In this case, changes in varactor bias cause a shift in phase of the reflection coefficient in the main line, but no change in VSWR. Actually some small fixed reflections may be present from the receiver circuit, the directional coupler, and from connector discontinuities. These fixed reflections will displace the small reflection coefficient circle away from the origin as shown for example in Fig. 5 and result in the varactor changing the VSWR in the main line. It can be deduced from the diagram that a relatively small offset of this small reflection coefficient circle will not significantly affect the maximum drift sensitivities calculated from Eqs. (18) and (19). Nor will it greatly affect the values of ψ_L at which maximum effects occur. However, an offset comparable to radius of the reflection coefficient circle can have a significant effect. It can also be deduced from Fig. 5 that if a drift of magnitude or phase of the offset occurred, it would produce a drift of $|\Gamma_L|$ or ψ_L even though the varactor tuning was fixed.

Acknowledgement

Technical discussions with and contributions from Dr. W. Higa and R. Clauss are gratefully acknowledged.

References

1. Moreno, T., *Microwave Transmission Design Data,* Dover Publications, Inc., New York, 1948.

2. Vessot, R. F. C., et al., "Recent Developments Affecting the Hydrogen Maser as a Frequency Standard," in Final Report prepared for NASA entitled *Research and Development For a Ground-Based Hydrogen-Maser System,* Smithsonian Institute, Astrophysical Observatory, Cambridge, Mass., April 1972.

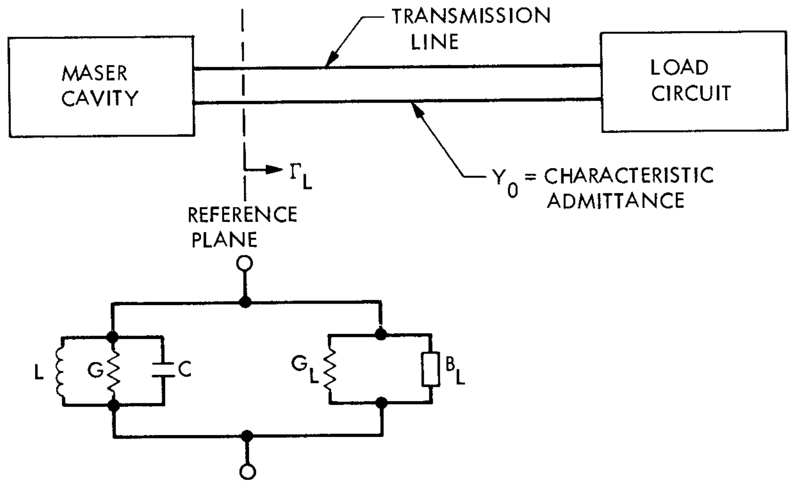

Fig. 1. Maser oscillator and load and equivalent lumped circuit

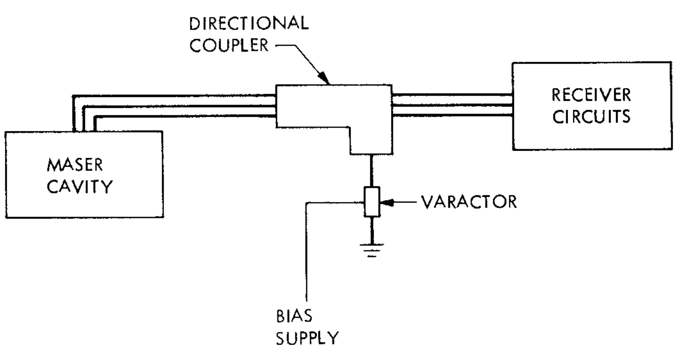

Fig. 2. Output circuit of maser oscillator

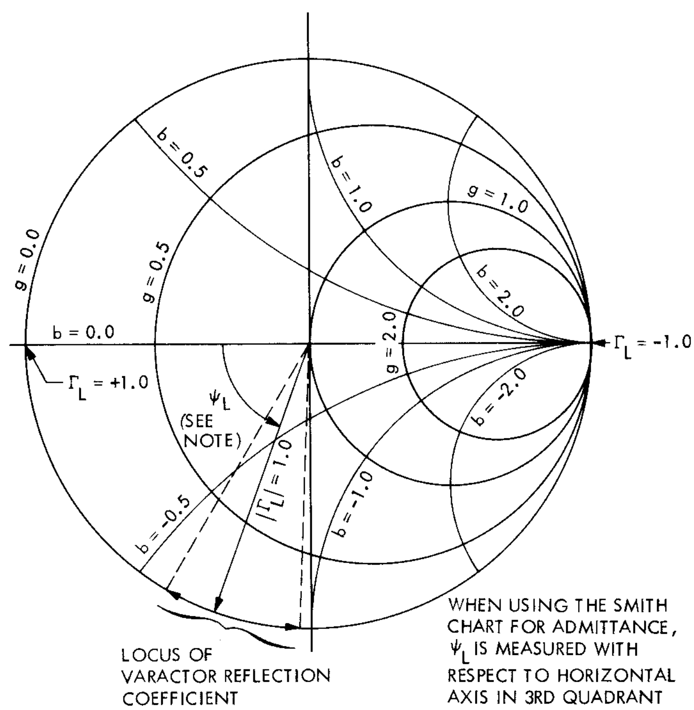

Fig. 3. Admittance and voltage reflection coefficient diagram for varactor

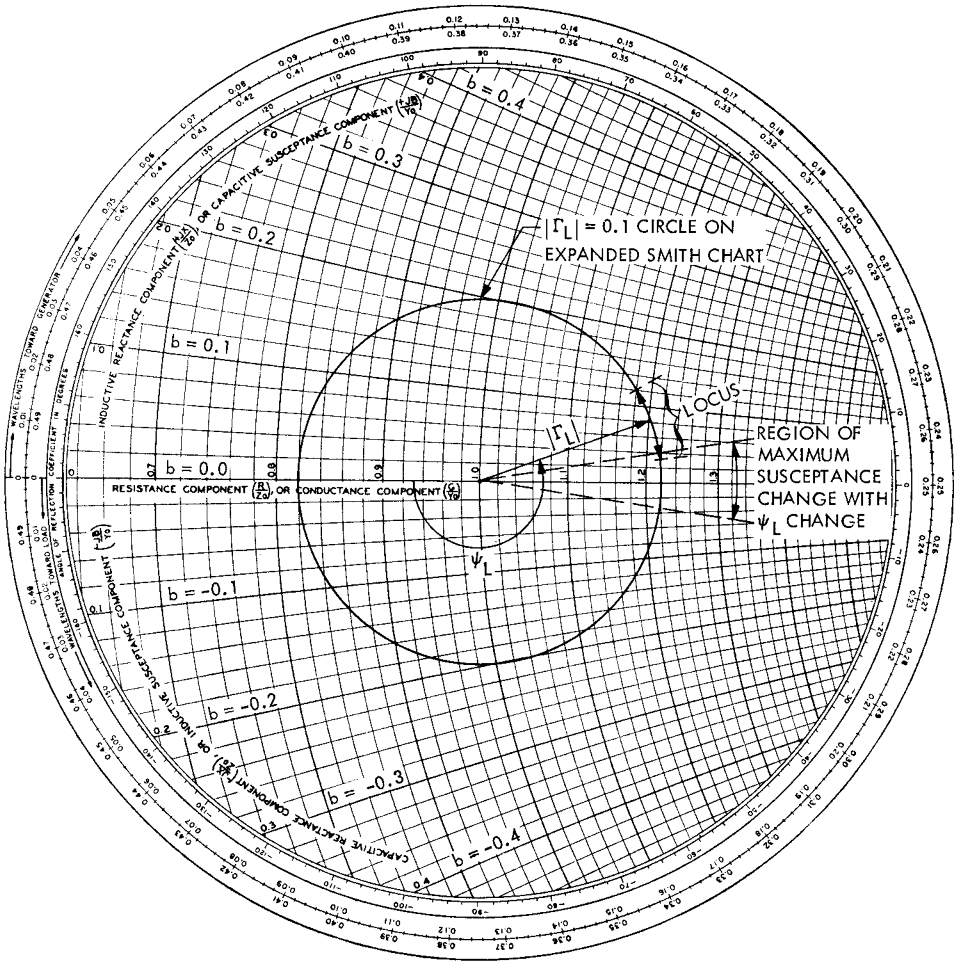

Fig. 4. Locus of varactor reflection coefficient variation in main line of directional coupler

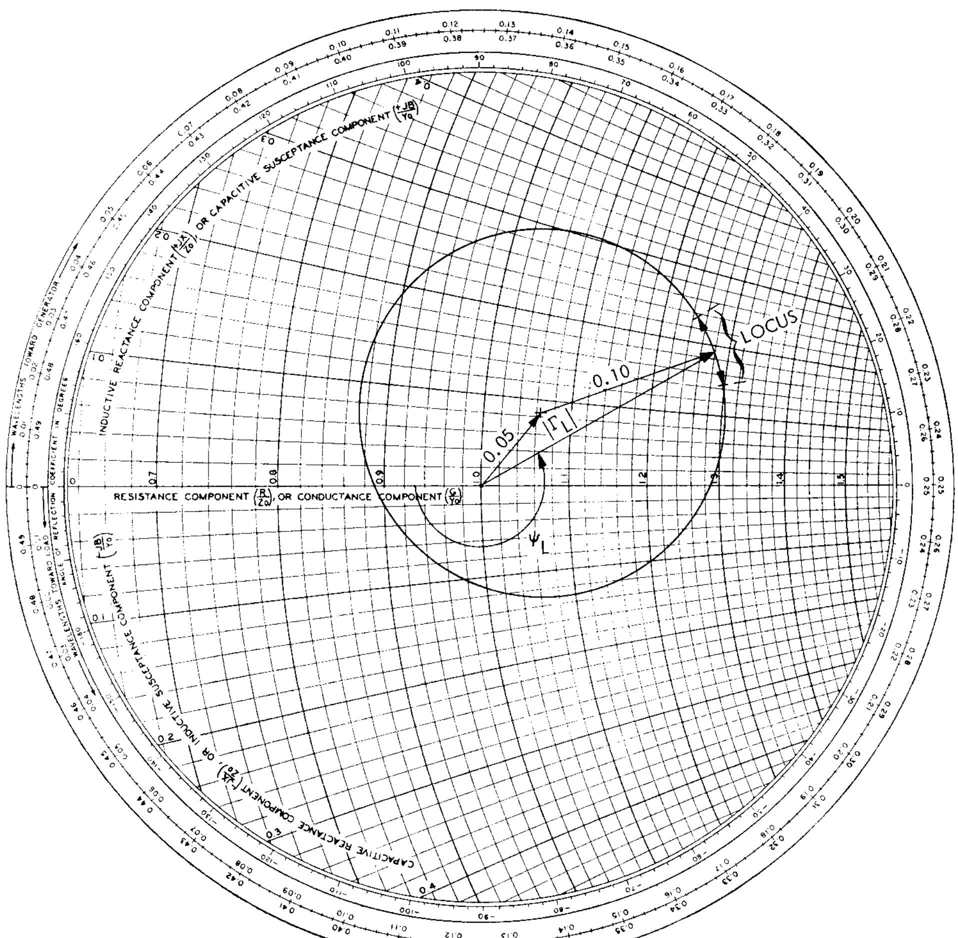

Fig. 5. Offset reflection coefficient locus of varactor as seen in main line